DYNAMICS OF FLUORESCENCE MARKER CONCENTRATION AS A PROBE OF MOBILITY

D. E. KOPPEL, D. AXELROD, J. SCHLESSINGER, E. L. ELSON, *and* W. W. WEBB

From the School of Applied and Engineering Physics, Department of Chemistry, Cornell University, Ithaca, New York 14853. Dr. Koppel's present address is the Department of Biochemistry, University of Connecticut Health Center, Farmington, Connecticut 06032.

ABSTRACT We have developed an effective experimental system for the characterization of molecular and structural mobility. It incorporates a modified fluorescence microscope geometry and a variety of analytical techniques to measure effective diffusion coefficients ranging over almost six orders of magnitude, from $<10^{-11}$ cm^2/s to $>10^{-6}$ cm^2/s. Two principal techniques, fluorescence correlation spectroscopy (FCS) and fluorescence photobleaching recovery (FPR), are employed. In the FPR technique, translational transport rates are measured by monitoring the evolution of a spatial inhomogeneity of fluorescence that is produced photochemically in a microscopic volume by a short burst of intense laser radiation. In contrast, FCS uses laser-induced fluorescence to probe the spontaneous concentration fluctuations in microscopic sample volumes. The kinetics are analyzed by computing time-correlation functions of the stochastic fluctuations of the measured fluorescence intensity. The optical system and digital photocount correlator designed around a dedicated minicomputer are described and discussed. The general power of these techniques is demonstrated with examples from studies conducted on bulk solutions, lipid bilayer membranes, and mammalian cell plasma membranes.

INTRODUCTION

In recent years a number of modern optical techniques, intensity fluctuation spectroscopy (IFS) (1, 2), fluorescence correlation spectroscopy (FCS) (3–6), and fluorescence photobleaching recovery (FPR, as we call our version of the technique) (7–12), have been developed to provide the capability of characterizing molecular transport (translational diffusion, electrophoresis, convective transport, cytoplasmic streaming, etc.) over distances down to the order of a wavelength of light. Such information can be seen to be of potential value from two complementary points of view. In studies of a molecular species in a known environment, the transport dynamics help to characterize molecular structure: size, shape, degree of aggregation. Alternatively, molecules of known characteristics can be used to probe an unknown environment. Under appropriate circumstances, moreover, these techniques are applicable to the kinetics of localized processes such as chemical reactions (2, 4, 12) and molecular rotational Brownian motion (2, 13, 14).

The first of these techniques, laser light scattering (IFS), has been applied with best success to highly purified solutions of biological macromolecules, measuring, predominantly, the molecular translational diffusion coefficients. While methods have been devised to separate (15) and analyze (16) some types of multicomponent samples, applications to complex biological systems have been limited by the lack of probe specificity.

In our ongoing studies of the lateral mobilities of molecular and structural components in planar lipid bilayer membranes (BLMs) and cell plasma membranes, we have turned to two techniques, FCS and FPR, which take advantage of the high sensitivity and specificity of fluorescent probes. Detailed results of these studies will appear elsewhere (10, 12, 17).[1] It is the object of this paper to provide a critical overview, presenting theoretical principles and experimental procedures and examples in sufficient detail to enable others to assess the applicability of the FCS and FPR techniques to problems of their own interst.

FCS AND FPR: GENERAL PRINCIPLES

Fig. 1 illustrates the basic approaches of the FCS and FPR techniques. In both, a laser beam is focused onto the sample (e.g., a fluorescently labeled membrane), usually

[1] Fahey, P. F., D. E. Koppel, L. S. Barak, D. E. Wolf, E. L. Elson, and W. W. Webb. Manuscript in preparation.

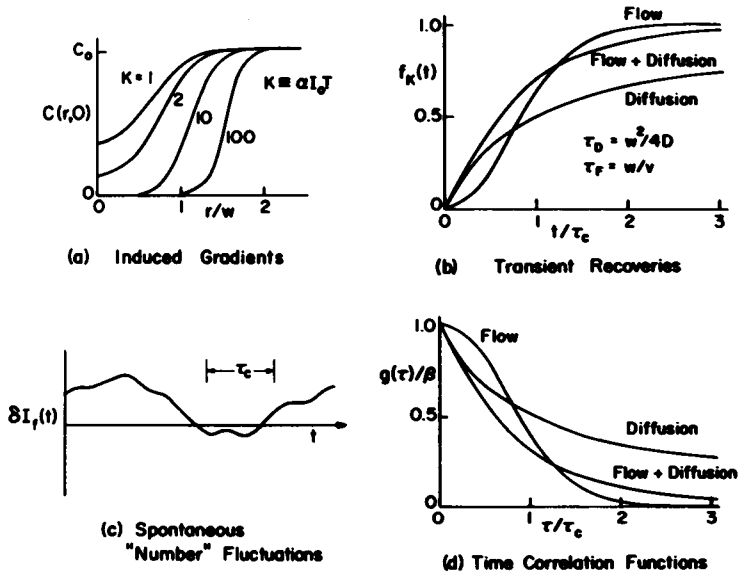

FIGURE 1 Basic principles. FPR: (*a*) Concentration gradients established by photochemical bleaches of various intensity. w is the $1/e^2$ radius of the Gaussian laser beam profile; C_o is the uniform concentration before bleaching. (*b*) Fractional fluorescence recoveries, in the low bleaching ($K \ll 1$) limit, calculated for diffusion ($\tau_c = \tau_D \ll \tau_F$), flow ($\tau_c = \tau_F \ll \tau_D$), and a mixture of the two ($\tau_c = \tau_D = \tau_F$). FCS: (*c*) Typical fluorescence number fluctuations. (*d*) Normalized correlation functions for diffusion ($\tau_c = \tau_D \ll \tau_F$), flow ($\tau_c = \tau_F \ll \tau_D$), and a mixture of the two ($\tau_c = \tau_D = \tau_F$).

to a diffraction limited spot of ~ 1 μm, and the emitted fluorescence is measured as a continuous function of time. With the FPR technique, transport dynamics are measured by monitoring the transient behavior of an inhomogeneous distribution of concentration. A brief exposure (brief compared to characteristic transport times) with a high laser power irreversibly bleaches the fluorophore within the beam, producing the spatial distributions of fluorophore shown in Fig. 1*a* for a Gaussian laser beam profile with $1/e^2$ radius w. The amount of bleaching, expressed as a parameter K, depends on I_0, the laser intensity at the center of the beam, T, the duration of the bleaching pulse, and α, the product of the fluorophore extinction coefficient and quantum efficiency of bleaching.

After bleaching, the recovery of fluorescence due to the redistribution of intact fluorescent chromophore is monitored with the same laser beam appropriately attenuated ($\times \sim 10^{-3}$–10^{-4}) to minimize further bleaching. Theoretical fluorescence recovery curves expressed as the fractional recovery, $f_K(t)$, are presented in Fig. 1*b* for diffusion, flow, and a combination of the two, calculated in the low bleaching (low K) limit. It is the object of data analysis to characterize the nature of the transport, and extract the characteristic times for diffusion, $\tau_D = w^2/4D$, and/or uniform velocity one-dimensional flow, $\tau_F = w/v$, where D is the diffusion coefficient, and v is the flow speed. A detailed account of FPR theory and data analysis procedures is presented in reference 11.

With the FCS technique, translational dynamics are characterized through the analysis of spontaneous stochastic fluctuations about equilibrium, without the imposition of a transient disturbance. The laser intensity is kept constant, but the fluorescence intensity, $I_f(t)$, changes nevertheless as molecules move relative to the laser beam, changing the number and distribution of molecules in the illuminated region (Fig. 1*c*). Analysis is performed with the computation of experimental estimates, $\hat{g}(\tau)$, of the normalized time autocorrelation function of the fluorescence intensity fluctuations,

$$g(\tau) \equiv <\delta I_f(t)\,\delta I_f(t+\tau)>/<I_f(t)>^2, \tag{1}$$

where $\delta I_f(t) \equiv I_f(t) - <I_f(t)>$, with the angular brackets indicating ensemble or finite run time averages. The extrapolated intercept, $\beta = <[\delta I_f(t)]^2>/<I_f(t)>^2$, the normalized variance of the intensity fluctuations, is of special interest in and of itself, for it provides an absolute determination of number density. For a monodisperse system (4),

$$\beta = 1/<N>, \tag{2}$$

where $<N>$ is the average number of independent fluorescent particles within radius w.

METHODS

Optics

A scheme of the basic optical system used for both types of experiments in our laboratory is presented in Fig. 2. The beam from an argon or krypton ion laser is directed by

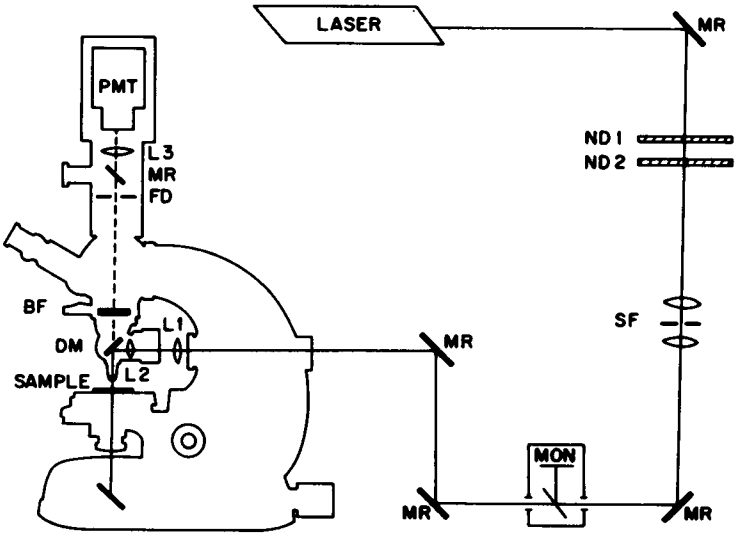

FIGURE 2 Optical schematic diagram for FPR and FCS experiments. *ND1, ND2,* neutral density filters; *SF,* spatial filter; *MR,* mirrors; *MON,* laser beam monitor; *L1, L2, L3,* lenses and microscope objectives; *DM,* dichroic mirror; *BF,* barrier filter; *FD,* field diaphragm in image plane; *PMT,* photomultiplier tube,

mirrors (*MR*) into the back of the vertical illuminator of a Zeiss Universal microscope. The laser intensity is attenuated with neutral density filters (*ND1* and *ND2*) to anything from $<1\ \mu W$ to >1 mW depending upon fluorophore photostability, laser beam size, and the type and characteristic time of transport. A spatial filter (*SF*) improves the Gaussian beam profile, removing high frequency spatial variations. *MON* is a light detector (PIN photodiode) used primarily in FCS experiments to monitor the laser intensity in order to correct for incident laser fluctuations (see Electronics below). Lens *L1* is an auxiliary microscope objective that adjusts the final position and focus of the laser beam at the sample. A dichroic mirror *DM* reflects the laser light down through the microscope objective *L2* (which thus acts as both the condensor and light collector) but allows the sample fluorescence to be transmitted up to the photomultiplier tube *PMT*. *DM* is thus in a position to act also as a barrier filter along with BF to block the back-scattered and reflected excitation light.

The dichroic mirror is exposed to the full incident laser power so that consideration must be given to its intrinsic photoluminescence as well as transmission spectrum. When standard dichroic reflectors proved unsatisfactory in either of these regards (the Zeiss FL500 reflector is adequate, the FL580 is not), we turned to special order optics (Pomfret Research Optics, Stamford, Conn.; Valtek Corp., Holliston, Mass.). The barrier filter, on the other hand, is exposed to only a small fraction of the laser power. Thus, while the photoluminescence of color filter glasses is considerable (18), standard sharp-cut yellow and red filters (Corning Glass Works, Corning, N.Y.; Schott Optical Glass, Inc., Duryea, Pa.) proved to be more than satisfactory.

In the FPR experiments, a light chopper is added to the laser beam. The bleaching pulse is produced by removing one of the neutral density filters with a solenoid (or even by hand in experiments with long characteristic transport times) for one period of the chopper cycle. This arrangement not only serves as a convenient way of timing the duration of the bleaching pulse, but also allows the attainment of shorter bleaching times than could be achieved with a solenoid-activated filter alone. The chopper duty cycle, moreover, reduces the extent of bleaching during the recovery phase of the experiment. One can thus monitor the recovery with a correspondingly higher laser power, reducing the effect of asynchronous background such as room light and dark current.

It is necessary to protect the PMT from the high level of fluorescence emitted during the bleaching pulse. This may be accomplished with a synchronous shutter or filter, or by pulsing down the PMT high voltage.

These experiments require a high degree of optical stability. If, for example, the laser beam moves relative to some limiting aperture, a systematic intensity variation will result. With a well-aligned system, however, this effect is ordinarily not serious in an FCS experiment, and is inconsequential in FPR, where much larger systematic fluctuations can be tolerated. Relative movements between the focused laser spot and the fluorescent sample present a more serious problem. The amplitudes of such movements must be kept much smaller than the beam size, w. To ensure this degree of stability, we have mounted the entire optical system on an optical table isolated from floor vibrations. Quantitative checks on our system, performed by measuring the correlation functions of laser light transmitted past a knife edge on the sample stage, show relative displacements of <0.03 μm, nearly two orders of magnitude smaller than w.

A field diaphragm or pinhole placed in the image plane (*FD* in Fig. 2) plays a vital role in discriminating against background fluorescence, i.e. fluorescence from regions other than the sample plane of interest. The way this is accomplished can be seen with the help of Fig. 3. Fluorescence from object point O_1, in the center of the in-focus object plane, is not obstructed by the diaphragm, while fluorescence from above or below or to the side (e.g., O_2) is obstructed to varying degrees.

To put this observation in a more quantitative form, we introduce the following definitions: $I(x) \equiv$ fluorescence excitation intensity distribution in object space; $G(x';x) \equiv$ light intensity at x' in image space from a point source of fluorescence at x in object space; $T(r') \equiv$ diaphragm transmission profile at the image plane ($z' = L$). We further define $\epsilon(x)$, a point source collection efficiency,

$$\epsilon(x) \equiv \int T(r')G(x';x)\,|_{z'=L}\,d^2r' / \int G(x';x)\,|_{z'=L}\,d^2r', \tag{3}$$

and $E(z)$, the collection efficiency of fluorescence excited in a plane by $I(x)$,

$$E(z) \equiv \int I(x)\epsilon(x)d^2r / \int I(x)d^2r. \tag{4}$$

We find that [for reasonably chosen functional forms of $I(x)$, $G(x';x)$ and $T(r')$, within limits described in the Appendix],

$$\epsilon(x) \simeq [1 + \tfrac{1}{2}(\Delta z/l)^2]^{-1} \exp\{-(r/s_o)^2[1 + \tfrac{1}{2}(\Delta z/l)^2]^{-1}\}, \quad (5)$$

where Δz and r are the distances of the point source from the in-focus object plane and the optic axis, respectively, s_o is the radius of the field diaphragm imaged onto the object plane (i.e. the actual radius divided by the magnification of the objective), and

$$l = s_o \cot \alpha_o, \quad (6)$$

where α_0 is the collection half angle of the objective (see Fig. 3). When the sample is illuminated with a focused laser beam parallel to the optic axis,

$$E(z) \simeq [1 + (\Delta z/l)^2]^{-1}. \quad (7)$$

In this case, the fluorescence collection efficiency (see Fig. 3) is sharply peaked about the in-focus object plane. Actual measurements of $E(z)$ agree with Eq. (7) quite well. If, however, the sample is uniformly illuminated with a conventional light source over a radius $\gg s_o[1 + \frac{1}{2}(\Delta x/l)^2]^{1/2}$, $E(z)$ is independent of z.

The significance of the result embodied in Eq. (7) can be appreciated by considering the case of a tissue cell in culture adhering to a substrate. Both the substrate and

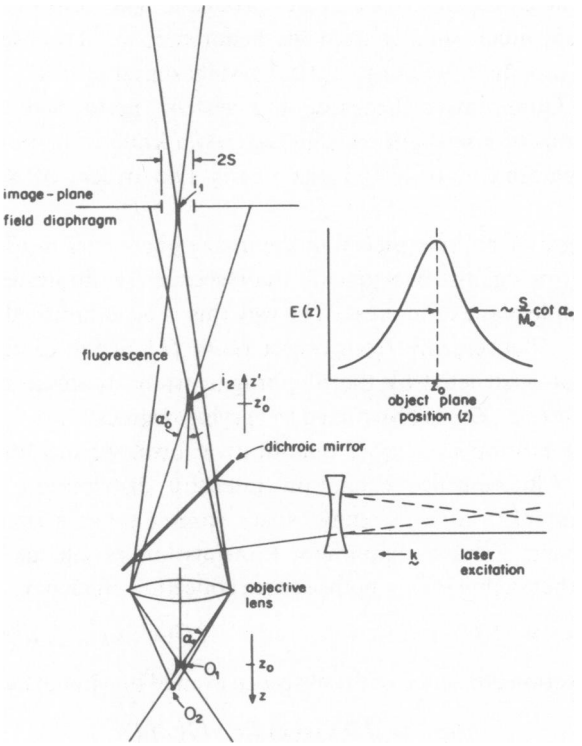

FIGURE 3 Optical ray diagram of collection selectivity produced by field diaphragm in image plane. M_o is the magnification of the microscope objective.

growth medium will fluoresce to an extent over which one does not always have complete control. For either, however, one collects the fluorescence only from a thickness equivalent to

$$\int_o^\infty E(\Delta z)d\Delta z \simeq \pi l/2. \tag{8}$$

For even a moderate power objective (e.g., × 40, 0.75 NA water), l can be made to be only ~ 10 μm, so that background fluorescence can be kept to a manageable level.

The collection efficiency profile can also be used in bulk solution experiments to define optically the effective thickness of the sample. This would be especially advantageous for molecules with a strong tendency to adhere to glass surfaces.

Electronics

The output of the PMT (RCA C31034A in a dry ice-cooled housing) is first processed (PAR 1120 amplifier-discriminator) to produce a series of uniform pulses, each corresponding to the detection of a single photon. This signal, together with the analog output of the laser beam monitor (MON), is fed into the array of digital circuitry diagrammed in Fig. 4. The net result is a continuous series of 16-bit binary numbers, $n(t_i)$, each corresponding to the number of photocounts in a counting interval starting at t_i, normalized for incident laser intensity fluctuations. The data sampling periodicity ($t_{i+1} - t_i = \tilde{M}\mu s$) is adjusted with thumbwheel switches connected to the $\div\tilde{M}$ circuits (Motorola MC 4016). Compensation for laser intensity changes is accomplished, as shown, by gating the counter summing the photocount pulses with the output of a binary circuit set by a crystal oscillator clock, and reset after a fixed num-

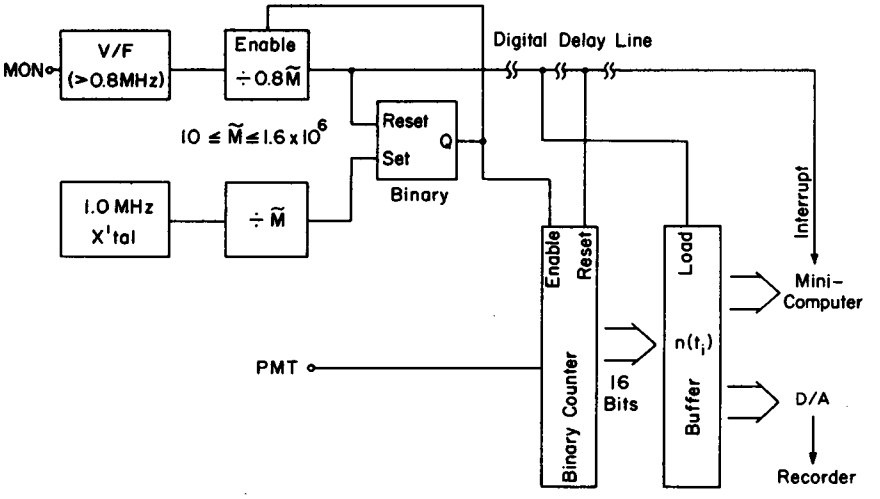

FIGURE 4 Schematic diagram of digital electronics, featuring circuitry correcting for incident laser fluctuations. *V/F* and *D/A* signify voltage-to-frequency and digital-to-analog converters, respectively. The $\div\tilde{M}$ circuits (Motorola MC 4016) put one pulse out for every $\tilde{M}$ pulses in.

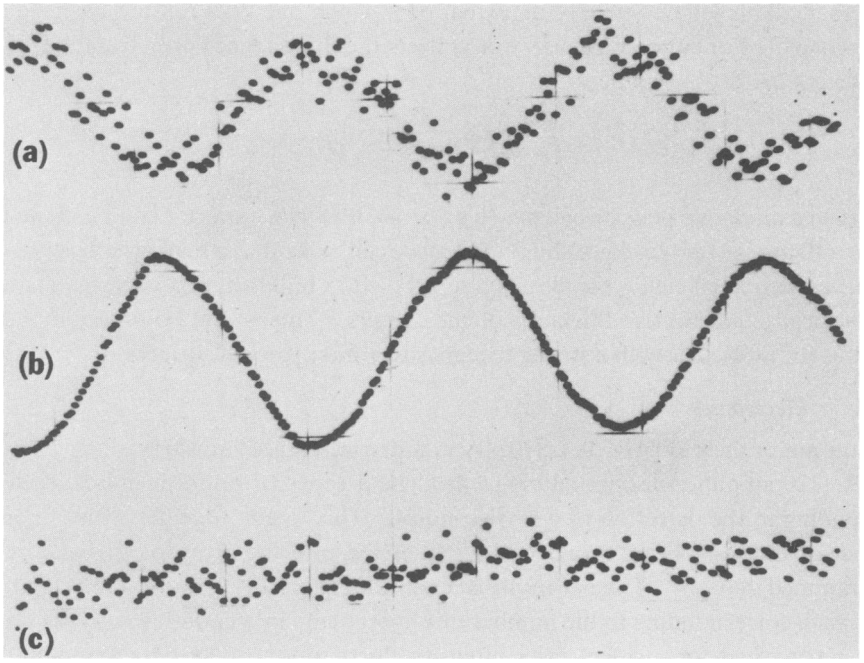

FIGURE 5 Oscilloscope traces of D/A output demonstrating correction for variations of laser intensity. (*a*) With correction disabled, fluorescence photocounts excited by sinusoidally modulated (1.0 Hz, 2% peak-to-peak) laser intensity. (*b*) Modulated counting interval widths of enabled correction circuit shown counting constant frequency (10 MHz) oscillator. Note 180° phase shift. (*c*) Same as (*a*), but with correction enabled.

ber (0.8 $\tilde{M}$) of periods of a voltage-to-frequency converter (Teledyne-Philbrick 470501, 1 MHz V/F) driven by the MON signal. Fluorescence photocount pulses are thus summed over intervals corresponding to a constant integrated laser intensity. Once the monitor load resistor is adjusted to give a V/F output of >0.8 MHz, the normalization circuitry is set for any data repetition rate (any value of $\tilde{M}$). The operation of the normalization circuitry is demonstrated in Fig. 5.

FPR transients are recorded on a strip chart recorder or transient recorder, and analyzed by the methods of reference 11. Normalization of laser fluctuations is not ordinarily required.

FCS digital data is transferred directly to a dedicated minicomputer (PDP 11-20) for further processing. Computer software constructs and displays the photocount autocorrelation function (see reference 6) in real time, and completes the analysis with least-squares fits at the conclusion of each run. This system provides capabilities not available with commercial hard-wired correlators. Processing here is 100% digital for maximum efficiency, with a 16 bit per counting interval capacity to handle the high number of counts per correlation time needed to achieve good statistical accuracy in an FCS experiment (6). A software correlator, moreover, allows great flexibility in the data processing. Our program sums the correlation signals (reference 6, Eq. [6])

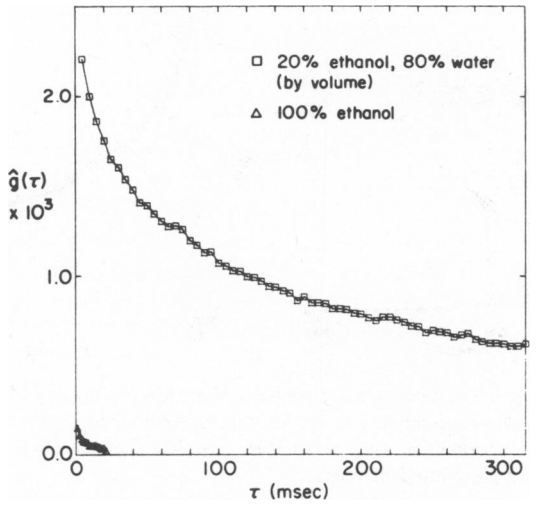

FIGURE 6 Fluorescence photocount autocorrelation functions of dilute solutions (8.0×10^{-9} g/ml) of dil dye in water-ethanol mixtures, 23°C.

computed in subdivisions of the total run time. This procedure effects a kind of high-pass digital filtering, reducing the contribution of slow systematic drifts. To avoid distorting the signal of interest, the run subdivisions are kept long ($\times \sim 10^3$) compared to the transport correlation time.

EXPERIMENTAL EXAMPLES

Bulk Solution

Fig. 6 demonstrates the type of information that one can obtain with the FCS technique. The functions shown are experimental estimates, $\hat{g}(\tau)$, of the normalized autocorrelation function (Eq. [1]), determined with dilute solutions (8.0×10^{-9} g/ml) of 3,3′-dioctadecylindocarbocyanine iodide (dil) in water-ethyl alcohol mixtures, prepared in 50 μm pathlength optical cells (Vitro Dynamics, Inc., Rockaway, N.J., "microslides"). Each dil molecule has a polar head group and two 18-carbon aliphatic tails, very much like a membrane phospholipid. It has been extremely useful to us as a probe of the lipid matrix of both model BLMs (see footnote 1 and discussion below) and mammalian cell membranes (10, 12, 17). We incorporate it into cell membranes, in fact, via dispersions of alcohol solutions in aqueous buffer (0.5–2.0% ethyl alcohol). The nature of these dispersions can be appreciated with reference again to the curves of Fig. 6. The dramatic difference between the two curves (recall: $\beta = 1/\langle N \rangle$; $\tau_D = w^2/4D$) indicates the formation of large dye aggregates in the predominantly aqueous solvent. From the intercepts and correlation times of such functions, one can obtain directly the average molecular weight and size (hydrodynamic radius) of particles in an aggregating system.

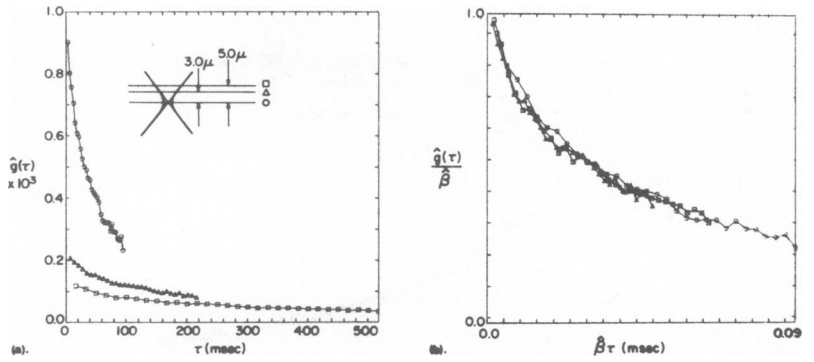

FIGURE 7 Fluorescence photocount autocorrelation functions of dil dye in a BLM at 12°C formed from a 1:2 molar ratio mixture of egg lecithin:7,dehydrocholesterol in octane. (*a*) Measured, as indicated, with different laser beam sizes. (*b*) The same functions, each normalized and scaled by $\hat{\beta}$, its computer-fitted intercept.

Model BLMs

The experiments depicted in Fig. 7 were performed on a single egg lecithin-cholesterol BLM (2:1 molar ratio) formed on a platinum wire loop, with a mole fraction of dil of $\sim 10^{-3}$ added to the membrane-making solution.[1] Measurements were made with a ×40 water immersion objective placed directly in the aqueous buffer surrounding the membrane. The three correlations functions in Fig. 7*a* correspond to three different beam sizes produced, as indicated, by moving the membrane relative to the focused laser beam. In a diffusion-controlled number fluctuation experiment, we recall,

$$\tau_D = w^2/4D,$$
$$\beta = 1/<N>$$
$$= 1/\pi w^2 \rho,$$

where ρ is the surface number density, so that

$$\beta\tau \propto \tau/\tau_D,$$

independent of w. That this is indeed the case for these data is demonstrated in Fig. 7*b*. Scaling the time axis of each curve by its calculated intercept, $\hat{\beta}$, produces the universal curve displayed here, corresponding to a diffusion coefficient of 9.9×10^{-8} cm^2/s.

Mammalian Cell Membranes

FPR has made its most notable contributions in the study of protein mobility in cell plasma membranes (7–10, 12, 17). The solid circles of Fig. 8 are recovery data of an L-6 (rat) myoblast incubated for 20 min in a solution of 5.0 μg/ml tetramethyl rhodamine-labeled succinyl Con A in Hank's balanced salt solution. Measurements were made with a ×40 water immersion objective placed directly in the aqueous buffer above the

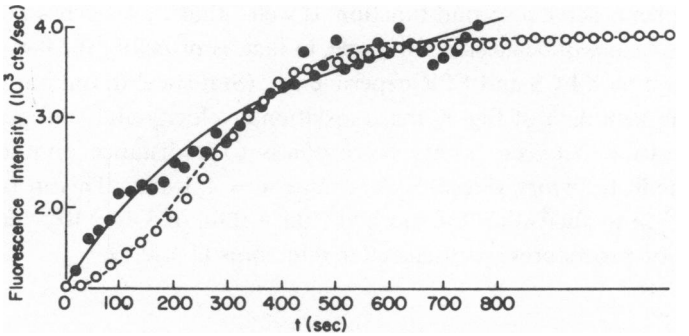

FIGURE 8 Fluorescence photobleaching recovery curves. Solid circles and solid line are L-6 rat myoblast data (cells are preincubated with 5.0 μg/ml tetramethyl rhodamine-labeled succinyl Con A, 23°C), and best-fit diffusion recovery theory. Open circles and dashed line are calibration scan (differential micrometer-driven scan of fixed fluorescently labeled Con A monolayer), and best-fit constant velocity flow recovery theory, scaled for qualitative comparison with the myoblast data.

cell adhering to a Falcon petri dish. The solid line is the best diffusion theory fit to the data (see reference 11) corresponding to a characteristic recovery time of 120 s.

For two reasons evident in Fig. 8, this measurement could not be made by the FCS technique. The characteristic time, first of all, is impossibly long. To get a correlation function of stochastic fluctuations with adequate statistical accuracy, it is necessary to average over many multiples of the characteristic time (6). The physiology of the cell evolves with time, however, so that for all practical purposes, FCS measurements are limited to correlation times of no more than 1 or 2 s. We have thus not been able to apply FCS to study membrane protein mobility, but we have used it to study the diffusion of dil incorporated into the lipid phase of cell membranes (10).

Second, there are large systematic fluorescence fluctuations, seen as a wavering of the recovery curve in Fig. 8, which overshadow the diffusion-controlled number fluctuations which form the basis of FCS. These systematic fluctuations are caused, we suspect, by the presence of immobile (nondiffusing on the time scale of the experiment) spatial inhomogeneities that are displaced by low amplitude undulations of the cell surface. The presence of this immobile protein fraction (shown by less than complete recovery of the fluorescence after bleaching) is, in fact, one of the most interesting results of our studies on cell membranes (10, 17).

An analysis of cooperative flow processes is also illustrated in Fig. 8. The open circles are data recorded by scanning with a differential micrometer through a bleached spot in a fixed, fluorescently labeled Con A monolayer. The dashed line is the theoretical fit of constant velocity flow recovery (11), scaled for qualitative comparison with the succinyl Con A-myoblast data. This comparison shows that the functional form of the myoblast data conforms much better with the theoretical curve for diffusion than with that for uniform flow.

Scan experiments serve a second function as well—that of laser beam size calibration. The uncertainty of beam size and shape, in fact, is probably the largest source of absolute error in both FCS and FPR experiments. (Statistical deviations are typically $\lesssim 10\%$.) In the scan data of Fig. 8, the translational velocity and time scale are such that the separation between points corresponds to a distance on the sample of 0.132 μm. The fit to theory gives a beam radius $w = 1.3$ μm. This in turn gives an effective diffusion coefficient for the succinyl Con A data of 3.4×10^{-11} cm^2/s. Other beam calibration procedures are discussed in references 11 and 19.

SUMMARY

The principal features of the FCS and FPR techniques are summarized in Table I. Although these two techniques probe substantially similar properties, each has its own advantages and limitations.

FCS is not practical for long correlation times, and is seriously limited by systematic fluctuations. Dye photochemistry is another potential problem. Only the most photostabile dyes can be used, and care must be taken to limit the laser intensity to a level at which photobleaching does not seriously affect the measured correlation function. FPR takes advantage of this photobleaching, but analysis can be made extremely difficult or impossible by complicated photochemical pathways, especially by a reverse chemical fluorescence recovery.

FCS gives the absolute number density, a fact which has recently been used to great advantage to determine molecular weights of large DNA molecules (20). FPR measurements give a direct quantitative determination of the presence of an immobile fluorescent component, a fact of potentially great physiological significance in studies of cell membranes (10, 12, 17). Together, as we have seen, they share powerful capabilities which should make major contributions in many areas of chemistry and biology.

TABLE I
SUMMARY OF PRINCIPAL FEATURES OF FCS AND FPR TECHNIQUES

	FCS	FPR
General nature	Stochastic concentration fluctuations	Photochemical perturbation
Probe	Fluorescent label	Fluorescent label
Data form	Correlation function	Transient recovery
Basic information	Molecular transport	Molecular transport
Additional information	Absolute number density	Immobile fraction
Limitations	(1) Systematic fluctuations (2) Time limitations (3) Photobleaching	(1) Chemical recovery (2) Sample damage

APPENDIX

Optics Collection Selectivity

For the purposes of this calculation (see Methods: *Optics* for motivation and essential definitions) we will sacrifice a certain amount of quantitative precision for the sake of analytical simplicity. We accordingly choose the following simple functional forms for $I(x)$, $G(x';x)$, and $T(r')$ which, although not rigorously correct (see reference 21) embody the essential geometrical features of the problem (see Fig. 3):

$$I(x) \propto [2/\pi w^2(z)] \exp[-2r^2/w^2(z)], \tag{A1}$$

$$G(x';x) \propto [2/\pi\sigma^2(z')] \exp[-2\,|\,r' - \Delta r'(x,z')\,|^2/\sigma^2(z')], \tag{A2}$$

$$T(r') = \exp(-r'^2/s^2), \tag{A3}$$

where $w(z)$, the $1/e^2$ radius of the incident laser beam focused (by an objective of radius a, focal length f, and convergent half-angle α_o) to a diffraction-limited spot size, w_o, in the in-focus object plane ($z = z_o$), is given by

$$w^2(z) = w_o^2 + (z - z_o)^2 \tan^2\alpha_o, \tag{A4}$$

where

$$z_o = Lf/(L - f), \tag{A5}$$

$$\tan\alpha_o = a/z_o; \tag{A6}$$

and where

$$\Delta r' = (z'/z)r \tag{A7}$$

$$\sigma^2(z') = \sigma_o^2 + (z' - z_o')^2 \tan^2\alpha_o'; \tag{A8}$$

where

$$z_o' = zf/(z - f), \tag{A9}$$

$$\tan\alpha_o' = a/z_o'. \tag{A10}$$

It then follows directly that

$$\epsilon(x) \equiv \int T(r')\,G(x';x)\,|_{z'=L}\,d^2r' \Big/ \int G(x';x)\,|_{z'=L}\,d^2r'$$
$$= [1 + \sigma^2(L)/2s^2]^{-1} \exp\{-(Lr/zs)^2[1 + \sigma^2(L)/2s^2]^{-1}\}, \tag{A11}$$

and

$$E(z) \equiv \int I(x)\epsilon(x)d^2r \Big/ \int I(x)d^2r = \{1 + [\sigma^2(L) + (L/z)^2w^2(z)]/2s^2\}^{-1}. \tag{A12}$$

Now, for s, the field diaphragm radius in the image plane, much greater than the resolution limit, i.e.

$$s^2 \gg \sigma_o^2$$
$$s^2 \gg (L/z)^2 w_o^2.$$

[(L/z_o) equals M_o, the magnification of the objective] and for $\Delta z \equiv z - z_o$ much less than z_o, we have, finally,

$$\epsilon(x) \cong [1 + \tfrac{1}{2}(\Delta z/l)^2]^{-1} \exp\{-(r/s_o)^2[1 + \tfrac{1}{2}(\Delta z/l)^2]^{-1}\}. \quad \text{(A13)}$$

and

$$E(z) \simeq [1 + (\Delta z/l)^2]^{-1}, \quad \text{(A14)}$$

where

$$s_o = s/M_o, \quad \text{(A15)}$$

and

$$l = s_o \cot \alpha. \quad \text{(A16)}$$

The authors are pleased to acknowledge the contributions of Mr. Lawrence Barak to the BLM experiment reported here, and the expert technical assistance of Mr. Richard Cochran and Mr. James Harman with the computer software and interface hardware. This work was supported by National Institutes of Health grant no. GM-21661, the National Science Foundation Division of Condensed Matter, European Molecular Biology Organization; travel grant to J. Schlessinger, National Institutes of Health Postdoctoral Fellowship NS-00432A to D. Axelrod, National Institutes of Health Career Development Award to E. L. Elson, Guggenheim Fellowship to W. W. Webb, and a grant from the Research Corporation, New York 10017.

Received for publication 11 June 1976.

REFERENCES

1. CARLSON, F. D. 1975. The application of intensity fluctuation spectroscopy to molecular biology. *Annu. Rev. Biophys. Bioeng.* **4**:243–264.
2. BERNE, B. J., and R. PECORA. 1976. Dynamic Light Scattering. John Wiley & Sons, New York.
3. MAGDE, D., E. L. ELSON, and W. W. WEBB. 1972. Thermodynamic fluctuations in a reacting system—measurement by fluorescence correlation spectroscopy. *Phys. Rev. Lett.* **29**:705–708.
4. ELSON, E. L., and D. MAGDE. 1974. Fluorescence correlation spectroscopy. I. Conceptual basis and theory. *Biopolymers.* **13**:1–27.
5. MAGDE, D., E. L. ELSON, and W. W. WEBB. 1974. Fluorescence correlation spectroscopy. II. An experimental realization. *Biopolymers.* **13**:29–61.
6. KOPPEL, D. E. 1974. Statistical accuracy in fluorescence correlation spectroscopy. *Phys. Rev.* **A 10**: 1938–1945.
7. PETERS, R., J. PETERS, K. H. TEWS, and W. BÄHR. 1974. A microfluorimetric study of translational diffusion in erythrocyte membranes. *Biochim. Biophys. Acta.* **367**:282–294.
8. EDIDIN, M., Y. ZAGYANSKY, and T. J. LARDNER. 1976. Measurement of membrane protein lateral diffusion in single cells. *Science (Wash., D.C.).* **191**:466–468.
9. JACOBSON, K., E. WU, and G. POSTE. 1976. Measurement of the translational motion of concanavalin A in glycerol-saline solutions and on the cell surface by fluorescence recovery after photobleaching. *Biochim. Biophys. Acta.* **433**:215–222.
10. SCHLESSINGER, J., D. E. KOPPEL, D. AXELROD, K. JACOBSON, W. W. WEBB, and E. L. ELSON. 1976. Lateral mobility on cell membranes: mobility of concanavalin A receptors on myoblasts. *Proc. Natl. Acad. Sci. U.S.A.* **73**:2409–2413.
11. AXELROD, D., D. E. KOPPEL, J. SCHLESSINGER, E. ELSON, and W. W. WEBB. 1976. Mobility measurements by analysis of fluorescence photobleaching recovery kinetics. *Biophys. J.* **16**:1055–1069.

12. ELSON, E. L., J. SCHLESSINGER, D. E. KOPPEL, D. AXELROD, and W. W. WEBB. 1976. Measurement of lateral transport on cell surfaces. Proceedings of the National Cancer Institute Conference on New Approaches to the Role of Membranes in Neoplasia. In press.
13. EHRENBERG, M., and R. RIGLER. 1974. Rotational Brownian motion and fluorescence intensity fluctuations. *Chem. Phys.* **4**:390–401.
14. ARAGÓN, S. R., and R. PECORA. 1975. Fluorescence correlation spectroscopy and Brownian rotational diffusion. *Biopolymers.* **14**:119–138.
15. KOPPEL, D. E. 1974. The study of *E. coli* ribosomes by intensity fluctuation spectroscopy of scattered laser light. *Biochemistry.* **13**:2712–2719.
16. KOPPEL, D. E. 1972. Analysis of macromolecular polydispersity in intensity correlation spectroscopy: The method of cumulants. *J. Chem. Phys.* **57**:4814–4820.
17. SCHLESSINGER, J., D. AXELROD, D. E. KOPPEL, W. W. WEBB, and E. L. ELSON. 1976. Lateral transport of a lipid probe and labeled proteins on a cell membrane. *Science (Wash., D.C.).* In press.
18. TURNER, W. H. 1973. Photoluminescence of color filter glasses. *Appl. Optics.* **12**:480–486.
19. SUZAKI, Y., and A. TACHIBANA. 1975. Measurement of μm sized radius of Gaussian laser beams using the scanning knife-edge. *Appl. Optics.* **14**:2809–2810.
20. WEISSMAN, M., H. SCHINDLER, and G. FEHER. 1976. Determination of molecular weights by fluctuation spectroscopy: application to DNA. *Proc. Natl. Acad. Sci. U.S.A.* **73**:2776–2780.
21. YOSHIDA, A., and T. ASAKURA. 1974. Electromagnetic field near the focus of Gaussian beams. *Optik.* **41**:281–292.